RSC Advances

ROYAL SOCIETY OF CHEMISTRY

www.rsc.org/advances

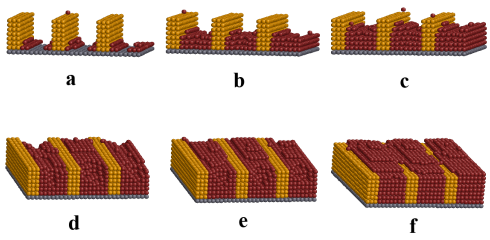

Three stages of step-edge induced selective growth were proposed: step-edge induced growth, layer-by-layer growth and central nucleation growth.

Step-edge induced area selective growth: A kinetic Monte Carlo study

Heng Zhang,[a] Gang Liu,[a] Wenchong Wang,[b] Lifeng Chi,[b] Shiling Yuan[a*]

[a] *School of Chemistry and Chemical Engineering, Shandong University, Jinan 250199, P. R. China*

[b] *Physikalisches Institut, Westfälische Wilhelms-Universität Münster, Wilhelm-Klemm-Str. 10, Münster 48149, Germany*

Abstract Template directed growth of functional organic molecules is a recently developed technique to generate organic mirco/nano-structures on surfaces. Using templates of metal patterned substrate, two different mechanisms were observed: area selective nucleation on predefined patterns with molecules nucleated on top of patterns and step-edge induced area selective growth on the substrate. Till now, much work has been done to investigate the microscopic mechanism of the former one. However, little attention was paid to the later one. Here in this work, a series of kinetic lattice Monte Carlo simulations were conducted to get deeper insight into the microscopic mechanism of step-edge induced area selective growth. The time-resolved process of structure formation, relationship between nucleation control efficiency and template size, and different growth regimes were studied. The results agree well with experimental speculation while selecting appropriate interactions.

Keywords: kinetic Monte Carlo simulation, nanofabrication, area selective growth

* Corresponding authors: Fax: +86 531 88365896 *E-mail address:* shilingyuan@sdu.edu.cn (S. Yuan)

I. INTRODUCTION

Micro/nanofabrication of functional organic molecule films is of paramount importance owing to their intensive applications in electronics and opto-electronics.[1-8] Unfortunately, photolithography cannot simply be applied to organic materials because they are sensitive to ultraviolet, organic solvents and water that involved in the procedure.[9] Recently, an indirect way to pattern organic functional molecule films using photolithography has been proposed.[10-17] The technique uses patterned surfaces as templates to control nucleation of molecules and create organic structures at pre-determined areas. Upon carefully choosing molecule-substrate-template system, two area selective growth mechanisms, namely binding energy difference and step-edge induced area selective growth are proposed.[11] For binding energy difference induced area selective growth, the substrate surface is patterned with materials with which the organic molecules have binding energies different from that with the substrate, for instance, SiO_2 surface patterned with Au structures. The molecules can be controlled to grow on the top of Au structure due to higher affinity with the material. For step-edge induced area selective growth, a strong in-plane interaction between molecules, such as N,N-dioctyl-3,4,9,10-perylene tetracarboxylic diimide (PTCDI-C8), is required. With PTCDI-C8, the molecules first nucleate at the edge of the structures, and then grow laterally owing to the strong π-π stacking, forming molecule structures in-between the Au structures.

The mechanism of binding energy difference induced area selective growth has been examined successfully by Monte Carlo (MC) simulation.[18-20] In the simulation, Lenard-Jones (LJ) pair potentials are applied to mimic the Van de Waals interaction between molecules. In contrast to the alternative of a molecular dynamics simulation, the Monte Carlo algorithm is faster to deal with the time scale separation in normal physical systems (separation of time scales between the thermal vibration and microscopic processed), while MD spends most the time sampling fast vibrations rather than executing the slower jumps. Since the short-time ballistic movement of the molecules is not interested, the Monte Carlo algorithm can accurately model the

diffusive process of the molecules. The performed Monte Carlo simulation of binding energy difference induced area selective growth bridged the experiments with theory in a good consistence, leading to a deeper understanding of the growth procedure on a microscopic level. [21-23]

Although the experimental mechanism was proposed several years ago, theoretical treatments on step-edge induced area selective growth are rarely reported. Figure 1a shows a typical atomic force microscope (AFM) image of PTCDI-C8 grown on Au stripes patterned SiO_2 surface. The Au pattern were fabricated by standard lithographic procedure, and the PTCDI-C8 molecules were deposited under high vacuum at a substrate temperature of 170 °C with a growth rate of 1 nm/min. The AFM image shows a clear area selective growth of layered molecule films between Au stripes. The AFM profile (Figure 1b, labeled by the line in Figure 1a) further gives a terraced structure, suggesting a layer by layer growth mode of the molecules. Based on our experiments, the growth process was speculated as following: initially deposited PTCDI-C8 molecules diffuse over the substrate surface, either on Au pattern or on SiO_2 substrate, and nucleate at the edge of the Au pattern. The films will grow laterally owing to the strong π-π interaction between the molecules, leading to the layered PTCDI-C8 films on SiO_2 substrate that observed in Figure. 1a.

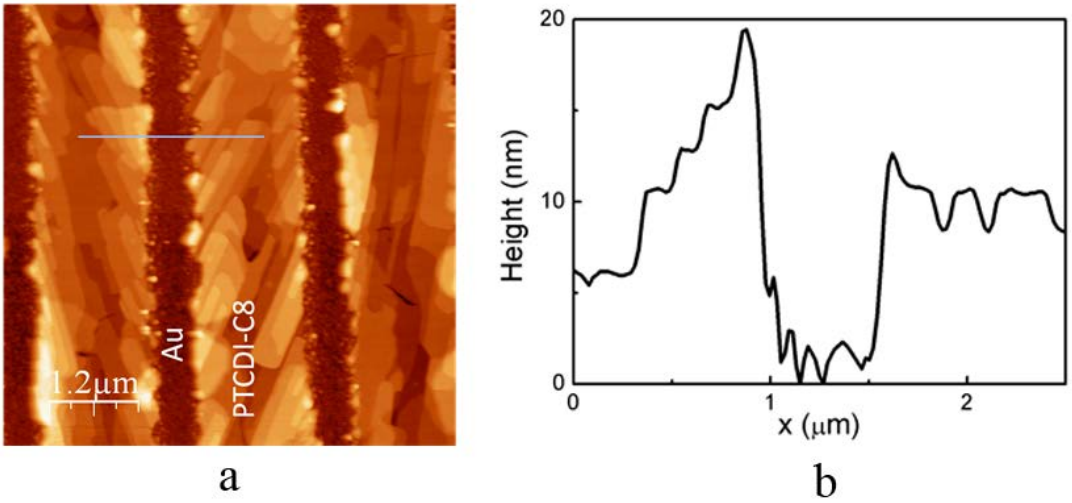

FIG. 1. Topographic AFM image a) and profile b) of PTCDI-C8 grown on Au stripes patterned SiO_2. The profile is measured on the line marked in a).

To gain deeper insight into the atomistic mechanism of step-edge induced area

selective growth, we examined the behavior of deposited particles on patterned substrate surfaces by means of kinetic lattice Monte Carlo simulations. The goal of the present work is to analyze the aggregation behavior of particles deposited on pre-patterned surfaces on a microscopic level, determine the relationship between nucleation control efficiency and template size, and find different growth regimes by tuning mutual interactions using a series of kinetic Monte Carlo simulations.

II. METHODS

A. Model

In the simulation, a two dimensional square lattice of size 30a×30a (a being the lattice constant) is built representing the SiO_2 substrate in the experiment. [24] Then stripes are built periodically on the substrate with a width of 3a, length of 30a and height of 8a (Figure 2) representing the stripe patterns in experiment. The thin film grows in z-direction, perpendicular to the substrate. As we are only interested in the growth and nucleation behaviors, all the molecules in the system are represented with spherical particles for simplicity.[20, 24] Periodic boundary conditions are applied in the x,y plane to yield a quasi-infinite surface. In the simulation, lattice Monte Carlo method based on a discretization of the problem is applied to improve computational efficiency. The method maintains the atomistic description of the system with much shorter simulation time. As a consequence, the accessible physical time scale and parameter range such as molecule beam flux were increased.

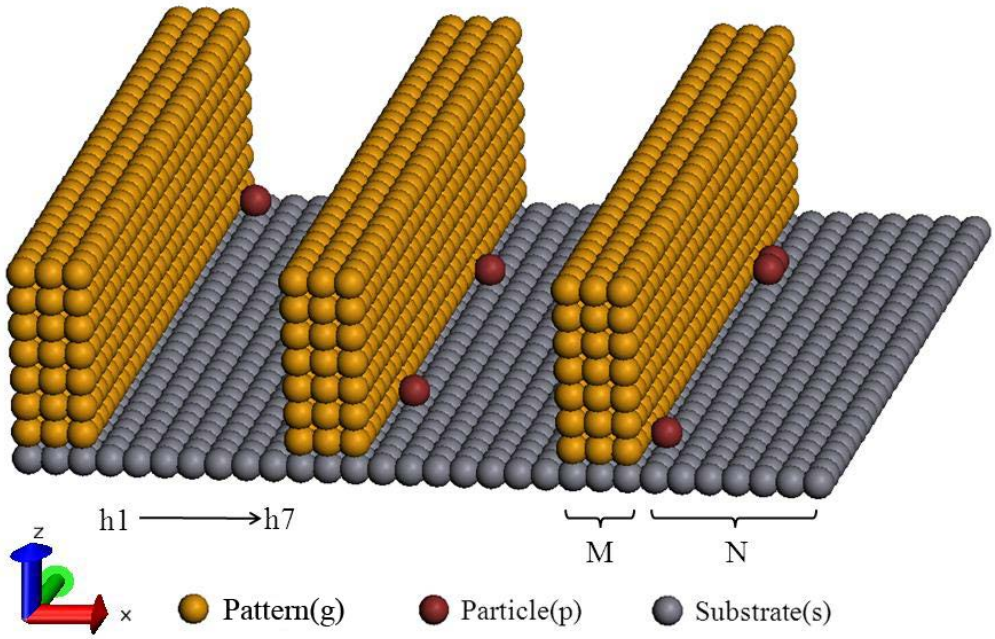

FIG. 2. Setup of simulation. The gray balls represent the substrate, the yellows stand for patterns, and the red reflect the deposited particles.

For computational efficiency, only the interactions between direct neighbor particles were considered. The cut-off distance then choose $\sqrt{3}a$ (i.e. the body diagonal distance of the cube crystal), above which the interaction energy can be neglected.[24] Since the substrate and stripe patterns are fixed, there are only three energy scales: deposited particle-deposited particle interaction ε_{pp}, deposited particle-pattern interaction ε_{pg} and deposited particle-substrate interaction ε_{ps}. Interaction between two arbitrary particles *i* and *j* of type *t(i)* and *t(j)* is given by:

$$E_{ij} = -\varepsilon_{t(i)t(j)} f(r_{ij}) \qquad (1)$$

where r_{ij} denotes the distance between particle i and j. $f(r_{ij})$ is defined as $f(r_{ij}) = 1$ for $r_{ij} \le \sqrt{2}a$, $f(r_{ij}) = 1/2$ for $r_{ij} = \sqrt{3}a$ and $f(r_{ij}) = 0$ for the else. In the simulation, ε_{ps}, ε_{pg}, and ε_{pp} is set to 0.3, 1.3 and 3.9 (unit k_BT) respectively.[24] The interaction energies were proved appropriate by Heuer in a similar research. By systematically vary ε_{pp} for fixed ε_{pg}=1.3, a very rich behavior of growth was detected. The deposited particle-substrate interaction ε_{ps} was set to 0.3 to assure a proper particle diffusion barrier on substrate while holds significant difference to the

interaction with stripes ε_{pg}. The deposited particle-deposited particle interaction ε_{pp} was set to 3.9 to mimic the strong interaction between them (such as the π interaction between PTCDI-C8 in the experiment).

B. Simulation details

In this study, the kinetic Monte Carol method is used to investigate the time evolution of the film growth. A list of all possible events that can occur in the system is constructed, including deposition and diffusion. Desorption is omitted since it is negligible under usual growth conditions.[25] During diffusion each particle can jump to the nearest neighbor sites with a probability p_i:

$$p_i = v_0 \exp(-E_b / kT) \tag{2}$$

where v_0 is the effective vibration frequency (taken to be 10^{13}/s for all cases in this work), E_b is the activation energy for the jump, k is Boltzmann's constant and T the temperature. Following Larsson's barrier model[26], the absolute value of the barrier E_b depends symmetrically on the energies of the old (E_μ) and the new (E_ν) state. The barrier E_b is expressed as:

$$E_b = \alpha(E_\mu + E_\nu) \tag{3}$$

where α is the weighting factor with a value 0.25886, which is derived from an analytical consideration of the relevant diffusion processes on the surface.[27]

During each Monte Carlo step, one event denoted by m is chosen psudo-randomly from all of the M events as given by:

$$\frac{\sum_{i=0}^{m-1} p_i}{\sum_{i=0}^{M} p_i} < N_R < \frac{\sum_{i=0}^{m} p_i}{\sum_{i=0}^{M} p_i} \tag{4}$$

where N_R is a random number, uniformly distributed between 0 and 1. If deposition is selected, then a particle is added to the system at random value of x, y and z *of* $h(x, y) + 1$. The simulation process is to model the continuous flux in the experiment. In our case, the flux corresponds to t_{flux} = 10 layers/sec. Much smaller fluxes would yield prohibitively long simulation time. After an event is performed, the clock will be advanced by time increment Δt, as given by:

$$\Delta t = \frac{-\ln(N_R')}{\sum_{i=1}^{M} p_i} \quad (5)$$

where p_i is the rate that event i occurs, and N_R' is another random number. The simulations are stopped after the deposition of 5400 particles.

Since we deal with stochastic processes, it is also important to average over different realizations. Over 10 independent realizations per data point are averaged for the figures shown in this work, which yields a sufficiently smooth behavior of the different realizations.

III. RESULTS AND DISCUSSION

A. Temporal evolution

Figure 3 shows the temporal evolution of particles deposited on patterned substrate surface. The film growth process can be clearly divided into three stages. In the first stage (Figure 3a), the deposited particles move along the surface searching for nucleation sites. Similar with the nucleation of atoms at atomic step that extensively observed, the step edges of the pattern with substrate provide preferential sites for particle nucleation. [28] Particles that initially deposited on surface, either on the substrate or the pattern, diffuse to the step-edges of the pattern within a few Monte Carlo steps. Following deposited particles can also diffuse to the topographically lower area namely the junction area of the substrate and the pattern immediately. The simulations further demonstrate that the deposited particles interact intensively with both the substrate and the pattern when reaching the junction. In the case, the diffusion of deposited particles is slowed down, resulting in a low hopping rate and high nucleation probability. Finally, the deposited particles are attached to the pattern edge, and providing new nucleation sites for the subsequent particles from diffusion or deposition. To sum up, the first stage growth suggests that step-edges of substrate and pattern play a crucial role for the growing of film in-between the patterns.

At the second stage (Figure 3b - 3d), even there is an energy barrier E_b aroused from interacting with the pattern for deposited particles detaching, they still have a

chance of $\nu_0 \exp(-E_b/k_BT)$ (v_0 can be interpreted as attempt frequency) to break the energy barrier and diffuse over the surface. During diffusion, these particles can be captured by nucleation sites of the layer below. Once nucleated there, it's hard to detach from surroundings cause the larger energy barrier E_b' aroused from the strong interaction between them. The deposited particles that attached to the patterns are then transported to the lower layer which leads to a lateral layer-by-layer growth.

One salient feature of Figure 1 is that no significant lateral growth of deposited particles on the pattern was observed, even when height of the film is much higher than that of the pattern. The phenomenon is also clearly demonstrated by the simulation, shown in Figure 3e to 3f of the third stage. The simulations show that particles have slower diffusivity when deposited on the central areas between neighbor patterns owing to the strong particle-particle interaction of ε_{pp}. The deposited particles can be immobilized there because of the large energy barrier created by the strong interaction of ε_{pp}. On the contrary, the particles deposited on the pattern have relatively faster diffusivity due to the weak interaction we set for the pattern and deposited particle of ε_{pg}. That is, deposited particles on the pattern have larger possibility to break the relative small energy barrier, and then diffuse to previously existed deposited particle region (i.e. the central areas between neighbor patterns), resulting in no significant lateral growth observed in experiments.

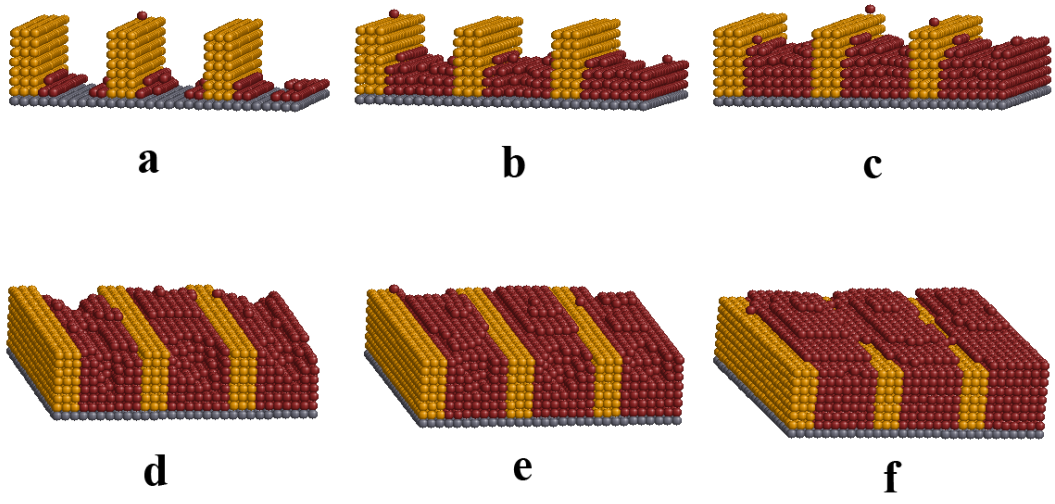

FIG. 3. Temporal snapshots of morphology evolution of particles deposited on patterned substrate

surface. The snapshots were taken after deposit a) 450 particles, b) 1800 particles, c) 2700 particles, d) 4050 particles, e) 4500 particles, f) 5400 particles. The ε_{pp} is set to 3.9.

Apart from the intuitive images from Figure 3, the film growth process can also be quantitatively reflected by tracking the height evolution of different growth stages and their standard deviations (Figure 4 and Figure 5). Here we adopt the number of deposited particles as the abscissa for convenience, although in principle one may also choose the time or Monte Carlo steps. For each pair (x, y), we define h(x, y) as z-component of particle which has maximum z value on the site. Correspondingly, h(x) = <h(x, y)> denotes the average height of deposited particles agglomerate at position x of the stripe pattern, e. g. h1 to h7 stand for the average heights of the sites between two neighbor stripe patterns in Figure 2. In Figure 4 and 5, we can see that h1, h7, h2 and h6 of sites near the stripe pattern increase rapidly with deposition time at the first stage, while h3, h4, h5 keep unchanged. The standard deviation also increases rapidly to 0.7 in this stage, which indicate deposited particles favor the step-edge areas, as illustrated in the inset of Fig. 4. After the deposition of 500 particles, all the heights begin to increase with a same rate and constant standard deviation. This reflects the second stage, the layer-by-layer growth stage. Apparently after the deposition of 5000 particles (the average height of central area exceeds over that of the stripe pattern), particles prefer to grow in the central areas between neighbor stripe patterns. This leads to a faster increase of height h3, h4, h5 than h1 and h7. These results are in good agreement with experiments in Figure 1 and the snapshots in Figure 2.

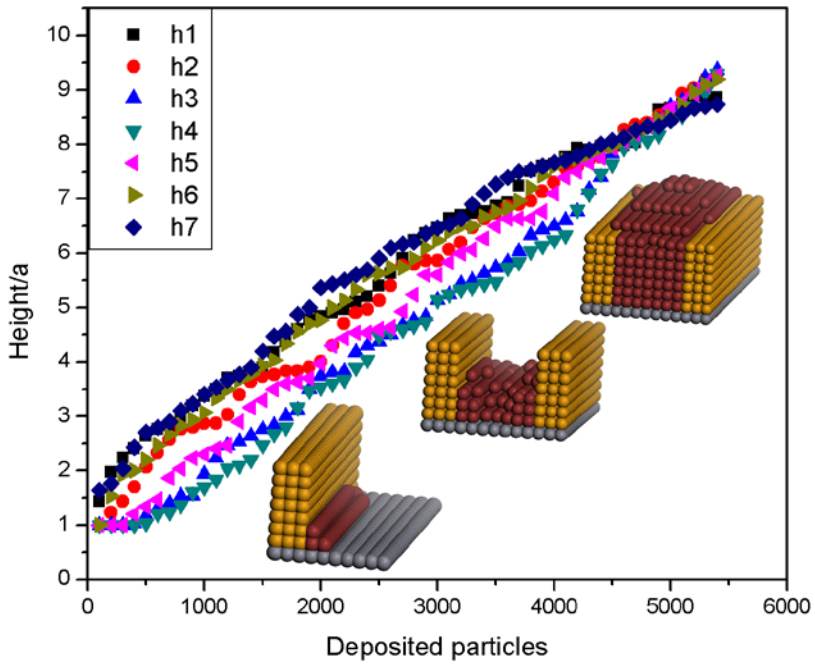

FIG. 4. Temporal evolution of height of h1 to h7. The insets show three different growth stages.

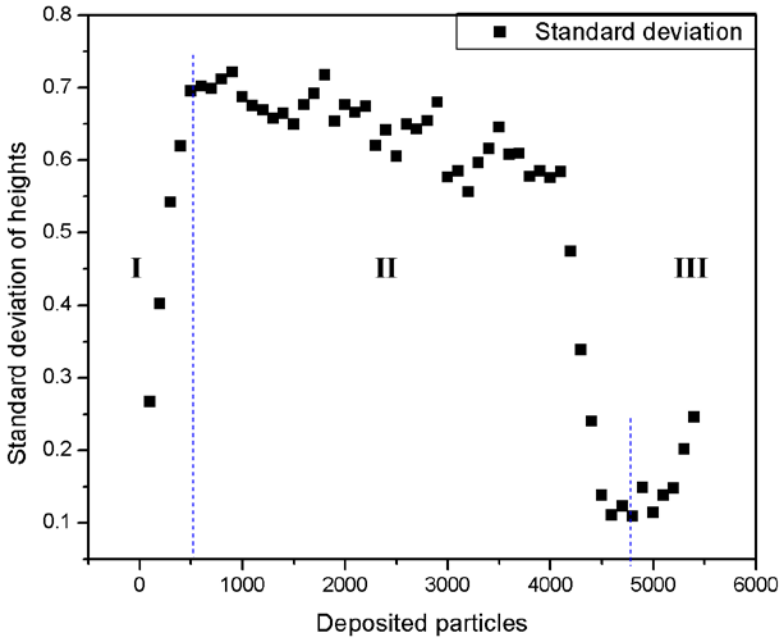

FIG. 5. Standard deviation of heights (h1 to h7) with evolution of deposited particle number.

B. Nucleation control efficiency

From an application point of view, one is interested in the maximal range of full nucleation control. Specifically this means: how far can (at constant deposition flux and temperature) the pre-patterned structures be placed without additional nucleation on undesired areas? Intuitionally, for a given molecule and substrate system, large

diffusion length resulting from high substrate temperature and low beam flux is favorable to achieve the full nucleation control. However, template sizes such as pattern width and period are also key parameters for nucleation control. The influence of template size on nucleation control is further quantified in the simulation. For a better description, we introduced nucleation control efficiency x_{NCE}. The x_{NCE} is defined as $N_{strip}/N_{cluster}$, where N_{stripe} and $N_{cluster}$ denote the number of stripe patterns and total number of clusters formed by deposited particles respectively. Any island that has more than 3 deposited particles is defined as a cluster. During the simulation, we only change the stripe width M and distance of two neighbor stripes N to investigate the relationship between nucleation control efficiency and template size by fixing the substrate temperature and beam flux.

First the stripe width M is kept at 3a. Increasing the distance between two neighbor stripes N, nucleation control efficiency x_{NCE} keeps nearly to unity when template period P (P=M+N) is smaller than 25a, indicating diffusion of deposited particles to the step-edges in a controlled way. However, when N is increased to above 22a (i.e. P>25a), nucleation control efficiency x_{NCE} drops linearly, suggesting that the distance is too large for deposited particles to arrive at step-edges. To investigate effect of stripe width M on the x_{NCE}, we take N at 20a. Similarly, x_{NCE} shows no change initially, and drops dramatically when the P exceeds 25a. This phenomenon can directly be used to explain the presence of crystalline grain on patterns with large width.[15] As shown in the simulation, the stripe width is a key parameter for the nucleation control efficiency. For large stripe width, the deposited particles cannot diffuse to the topographically lower area, nucleating stochastically with islands randomly distributed on the Au pattern.

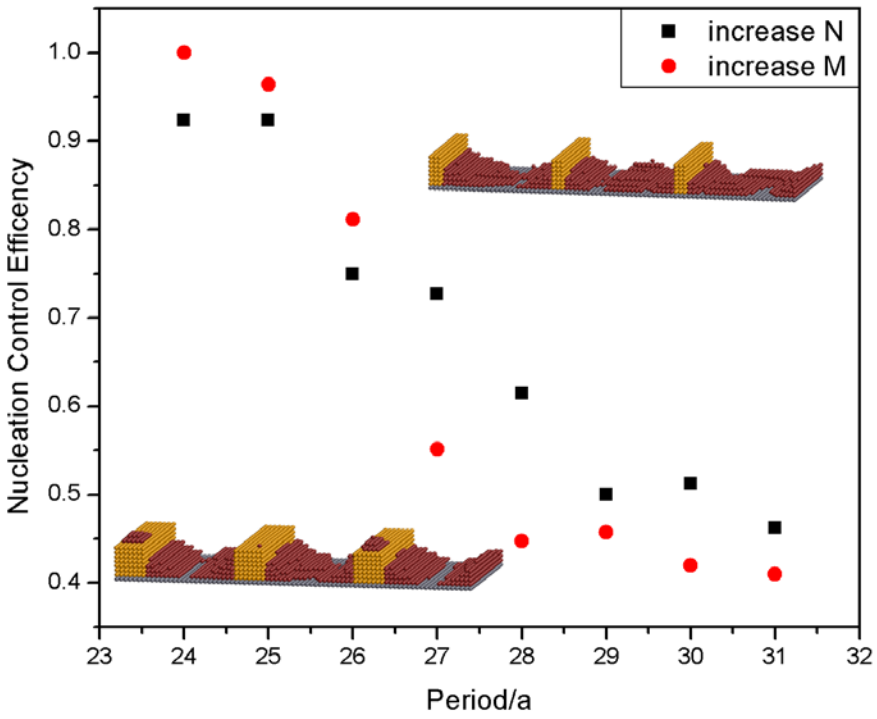

FIG. 6. Relationship between nucleation control efficiency x_{NCE} and template period P (P=M+N). Black squares: increasing N while keeping M unchanged (M=3a). Red circles: increasing M while keeping N unchanged (N=20a).

In conclusion, the full control of selective growth is not favored for large template size. Limited by diffusion length of deposited particles, the large size of template provides insufficient transport of the deposited particles to the predefined regions (e.g. step-edges of pattern and substrate). Additional clusters are then formed outside predefined areas (e.g. above the pattern, central area of the substrate). Full nucleation control can only be achieved under appropriate growth conditions (temperature and deposition rate) and appreciate template sizes.

C. Configurations as a function of ε_{pp}

So far the temporal evolution and nucleation control efficiency were investigated. It is also of interest to address the influence of particle-particle interaction on the evolution of morphology after the channels between patterns are filled. To quantify the effect of ε_{pp} on the final configurations, we introduced the coverage of deposited particles above patterns as a measurement of the area selective efficiency. In case all deposited particles grow in the area between neighboring patterns, we get the coverage ≈ 0. In the simulation, we vary the ε_{pp} from 0.5 to 3.9 with fixing ε_{pg}, ε_{ps} at

1.3, 0.3. For the large ε_{pp} of 2.7~3.9, most deposited particles diffuse to these areas with a small fluctuation of the coverage and very few particles stay above the patterns. From the visual inspection (Figure 7a), they resemble individual random nucleated agglomerates. The selective growth mainly induced by the high interaction energy between deposited particles (i.e. the slow diffusion on the central areas increased their nucleation probability). Under this situation full area selective growth control can be derived. With the decrease of ε_{pp}, the area selectivity begins to lose. Because the energy difference between ε_{pp} and ε_{pg} decreased. As a consequence, significant advancing of deposited particles onto patterns takes place. At very low ε_{pp} of about 0.9, there is even no selective growth owing to little energy difference for deposited particle on patterned area and existed particles area.

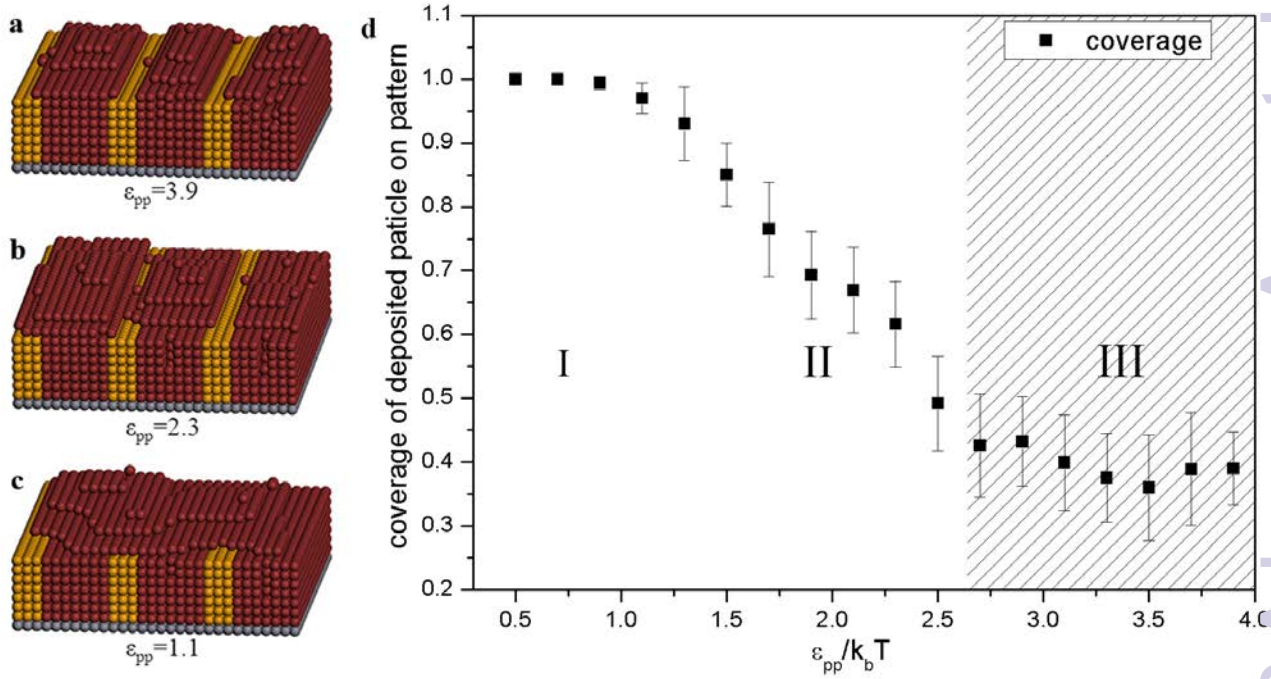

FIG. 7. The coverage of deposited particles above patterns in dependence of ε_{pp} and three typical configurations.

Three typical morphologies with ε_{pp} at 3.9, 2.3 and 1.1 are also shown in Figure 7 respectively. The three typical configurations lie right in the III, II, I region in Fig. 7d.With a strong particle-particle interaction of ε_{pp} at 3.9, the deposited particles will diffuse to the central areas between neighboring patterns, forming isolated clusters and leading to fully selective growth as shown in Figure 7a. Significant lateral growth

with deposited particles advancing to patterned area is observed as the ε_{pp} at 2.3, as shown in Figure 7b. With weaker particle-particle interaction of ε_{pp} at 1.1, the deposited particles start to cover the whole patterned area after filling the channels (Figure 7c). The three growth regimes were also found by experiments while selecting appropriate molecules (PTCDA, DtCDQA and NPB)[12,13,24].

IV. CONCLUSIONS

In conclusions, we investigated the film growth process, nucleation control efficiency and structure formation of particles deposited on pre-patterned substrates via a series of kinetic lattice Monte Carlo simulations. The film growth process can be clearly divided into three stages: step-edge induced area selective growth stage, layer-by-layer growth stage and central nucleation growth stage. In the first stage, deposited particles diffuse over the surface and nucleate at the edge of the Au stripes. In the second stage, the deposited particles follow a layer-by-layer growth regime to fill the topographically low layers for large mutual interaction energies. In the third stage, deposited particles tend to nucleate in the central areas owing to slow diffusivity there.

The relationship of template size and nucleation control efficiency is investigated. It turns out that increasing both the stripe's width and distance can reduce the nucleation control efficiency. Because of limited diffusion length of deposited particles over surface, large template size leads to insufficient transport of the deposited particles to the predefined areas, resulting additional island formation outside predefined regions. Finally, the morphology evolution dependence of ε_{pp} is examined through the coverage of deposited particles above patterns. By tuning ε_{pp} while keeping ε_{pg} and ε_{ps} fixed, three typical growth regimes are found. For the large ε_{pp}, particles cluster in the central areas between two neighbor patterns. The simulation results are in good agreement with experiments that no significant lateral growth happens even after the thickness of the organic layer exceeds the height of pattern. Decreasing ε_{pp} will lead to lateral growth of deposited particles onto the pattern, indicating a very strong particle - particle interaction is required for a

completely selective growth.

ACKNOWLEDGEMENT

We acknowledge the financial support by NSFC (No. 21173128). W. C. Wang and L. F. Chi would like to thank the financial support by the Transregional Collaborative Research Centre TRR 61 by the DFG and NSFC.

REFERENCES

1. X. Fang, Y. Bando, U. K. Gautam, C. Ye, and D. Golberg, *J. Mater. Chem.*, 2008, **18**, 509.

2. L. Bardotti, B. Prével, P. Jensen, M. Treilleux, P. Mélinon, A. Perez, J. Gierak, G. Faini, and D. Mailly, *Appl. Surf. Sci.*, 2002, **191**, 205.

3. S. Y. Chou, C. Keimel, and J. Gu, *Nature*, 2002, **417**, 835.

4. S. Lenhert, P. Sun, Y. Wang, H. Fuchs, and C. A. Mirkin, *Small*, 2007, **3**, 71.

5. J. Fan, J. Michalik, L. Casado, S. Roddaro, M. Ibarra, and J. De Teresa, *Solid State Commun.*, 2011, **151**, 1574.

6. S. L. Kim, and G. M. Kim, *Int. J. Precis. Eng. Man.*, 2011, **12**, 763.

7. Y. Bellouard, A. Said, M. Dugan, and P. Bado, *Opt. Express*, 2004, **12**, 2120.

8. S. R. Forrest, *Nature*, 2004, **428**, 911.

9. M. Cölle, M. Büchel, and D. M. de Leeuw, *Org. Electron.*, 2006, **7**, 305.

10. W. Wang, D. Zhong, J. Zhu, F. Kalischewski, R. Dou, K. Wedeking, Y. Wang, A. Heuer, H. Fuchs, and G. Erker, *Phys. Rev. Lett.*, 2007, **98**, 225504.

11. W. Wang, C. Du, D. Zhong, M. Hirtz, Y. Wang, N. Lu, L. Wu, D. Ebeling, L. Li, and H. Fuchs, *Adv. Mater.*, 2009, **21**, 4721.

12. W. Wang, C. Du, H. Bi, Y. Sun, Y. Wang, C. Mauser, E. Da Como, H. Fuchs, and L. Chi, *Adv. Mater.*, 2010, **22**, 2764.

13. W. Wang, C. Du, C. Wang, M. Hirtz, L. Li, J. Hao, Q. Wu, R. Lu, N. Lu, and Y. Wang, *Small*, 2011, **7**, 1403.

14. W. Wang, and L. Chi, *Acc. Chem. Res.*, 2012, **45**, 1646.

15. W. Wang, C. Du, L. Li, H. Wang, C. Wang, Y. Wang, H. Fuchs, and L. Chi, *Adv. Mater.*, 2013, **25**, 2018.

16. A. L. Briseno, J. Aizenberg, Y.-J. Han, R. A. Penkala, H. Moon, A. J. Lovinger, C. Kloc, and Z. Bao, *J. Am. Chem. Soc.*, 2005, **127**, 12164.

17. A. L. Briseno, S. C. Mannsfeld, M. M. Ling, S. Liu, R. J. Tseng, C. Reese, M. E. Roberts, Y. Yang, F. Wudl, and Z. Bao, *Nature*, 2006, **444**, 913.

18. F. Kalischewski, J. Zhu, and A. Heuer, *Phys. Rev. B.*, 2008, **78**, 155401.

19. F. Kalischewski, and A. Heuer, *Phys. Rev. B.*, 2009, **80**, 155421.

20. S. F. Hopp, and A. Heuer, *J. Chem. Phys.*, 2010, **133**, 204101.

21. A. C. Levi, and M. Kotrla, *J. Phys.: Condens. Matter*, 1997, **9**, 299.

22. H. Huitema, and J. Van der Eerden, *J. Chem. Phys.*, 1999, **110**, 3267.

23. K. A. Fichthorn, and W. H. Weinberg, *J. Chem. Phys.*, 1991, **95**, 1090.

24. F. Lied, T. Mues, W. Wang, L. Chi, and A. Heuer, *J. Chem. Phys.*, 2012, **136**, 024704.

25. L. Nurminen, A. Kuronen, and K. Kaski, *Phys. Rev. B.*, 2000, **63**, 035407.

26. M. I. Larsson, *Phys. Rev. B.*, 2001, **64**, 115428.

27. T. Michely and J. Krug, *Islands, Mounds and Atoms* Academic Press, Berlin, 2004.

28. D. G. de Oteyza, E. Barrena, M. Ruiz-Oses, I. Silanes, B. P. Doyle, J. E. Ortega, A. Arnau, H. Dosch, and Y. Wakayama, *J. Phys. Chem. C.*, 2008, **112**, 7168.